Analysis of Suspension System
Final Report
FEA 324 Sec: D

Abi Strait

Table of Contents

Memo

To: Jim Wong
From: Abi Strait
Date: December, 2025
Re: Analysis of Suspension System

MINES
Mechanical Engineering

Executive Summary

Problem Description and Project Goals

The project focused on the finite element modeling and design assessment of a front double-wishbone suspension corner. The main design goal was to reduce the mass of the lower control arm while still maintaining a minimum factor of safety of 3.5 against static failure under a representative combined vertical and horizontal wheel load. To do this, two finite element studies were run on the complete suspension assembly, and a separate, more detailed local analysis of the lower control arm was carried out to explore weight-reduction options while preserving the required safety margin. All major structural components in the assembly were modeled using AISI 4340 steel and cast carbon steel to reflect realistic strength, stiffness, and manufacturability for an automotive suspension application.

Approach and Analysis Methods

The suspension was analyzed using SolidWorks Simulation via several FEA (Finite Element Analysis) studies on the full assembly, along with an additional standalone study on the lower control arm. In both assembly models, the chassis connections for the upper and lower control arms were represented as fixed hinges, and all cylindrical joints were treated with pin connectors. A combined load was applied at the knuckle spindle, consisting of a 50 lbf vertical wheel load and a 100 lbf horizontal load, to approximate a severe in-plane operating condition. The model used three-dimensional tetrahedral solid elements with locally refined mesh in high-stress regions, and a mesh-convergence check was performed to ensure that changes in peak von Mises stress were within about 5%. Hand calculations for stresses and deflections were used alongside the FEA results to confirm that the numerical model was behaving as expected.

Key Findings and Outcomes

The combination of FEA and supporting analytical calculations produced consistent predictions of both stress and deflection for the suspension. Under the governing load case, the design meets the 3.5 factor-of-safety criterion, with the highest von Mises stresses concentrated in the lower control arm near the knuckle attachment, and wheel-center deflections remaining within reasonable limits. A follow-on design study on the lower control arm successfully reduced part mass while keeping the same load case and maintaining the required safety margin. The essential numerical outcomes are summarized in Table 1, and the final configuration demonstrates that the lower control arm can be lightened without sacrificing structural integrity or basic suspension performance.

Table 1: Simulation Results

Study Type	Max vonMises (kis)	Absolute x-normal stress (kis)	Max y-displacement (in)
Wishbone - fixed	17.64	-14.57	0.0041
Wishbone - Spring	17.65	-14.57	0.4504
Lower Control Arm	18.41	-15.23	0.00255

Background and Introduction

Context of the Suspension System and Design Intent

The system analyzed in this project is a rear double-wishbone suspension typical of a high-performance road car. It is made up of an upper control arm, a lower control arm, a steering knuckle, and a coil-over shock absorber, all tied back to the chassis through discrete hinge locations. Together, these components route combined vertical road loads and in-plane braking forces from the wheel hub through the knuckle and into the vehicle frame while still allowing controlled wheel travel and camber change, as sketched in Figure A.

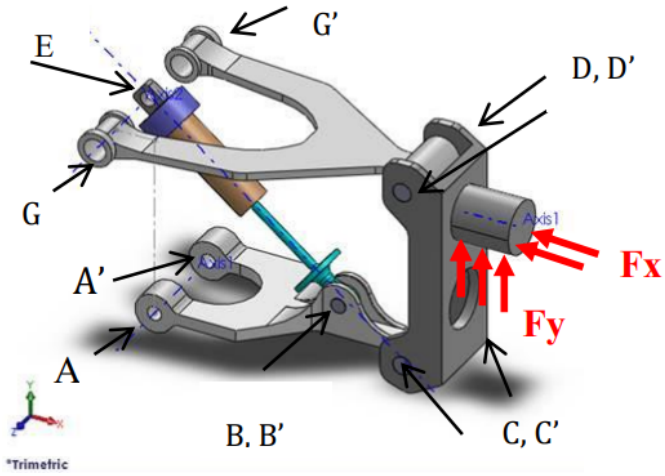

Figure A: Rear Suspension Assembly with points A-G

Within this study, the goal is to understand how this particular geometry and load path respond when the knuckle is subjected to a relatively severe in-plane load case. The focus is on whether the most highly loaded regions of the suspension—especially the lower control arm near the knuckle attachment and the shock mounting interfaces—can carry the applied forces without excessive stress or deflection. The broader design objective is to verify that these critical regions retain adequate strength and stiffness to support subsequent weight-reduction efforts on the lower arm and related components.

Design Constraints, Requirements, and Performance Targets

Under the prescribed spindle loading, the suspension must transmit forces into the chassis without local yielding, excessive elastic deformation, or significant loss of wheel alignment. In this report, performance is judged by comparing the peak von Mises stresses obtained from linear-elastic FEA to the corresponding material yield strengths, with an imposed minimum factor of safety. In parallel, vertical and lateral displacements at the knuckle and shock attachment points are monitored to ensure that predicted motions remain small relative to the available suspension travel. Special attention is given to geometric discontinuities—pin bores, fillets, and the shock-mount flange—because these areas are prone to stress concentrations and will largely dictate fatigue life under repeated loading.

Scope of Analysis and Modeling Assumptions

The numerical work is limited to the rear suspension corner defined in the project handout: the upper and lower control arms, knuckle, shock clamp, shock plunger, and shock tube. The remainder of the vehicle structure is represented through boundary conditions rather than explicit geometry: each frame mounting location is modeled as a hinge constraint, and the joints between the arms, knuckle, and frame are implemented with connector (pin) elements instead of fully modeled solid pins. This captures realistic load transfer at the joints while keeping the mesh size and contact definitions manageable.

The analyses are carried out as static, small-displacement, linear-elastic simulations. Dynamic effects, material nonlinearity (plasticity), thermal loads, residual stresses from manufacturing, and geometric imperfections are not included. Contact between parts is simplified as either ideal contact or bonded/connector interfaces, and all materials are taken as homogeneous, isotropic steels. Mesh refinement is concentrated in areas expected to experience large stress gradients—such as around bores, fillets, and shock-mount features—while less critical regions use a coarser mesh to control model size. These modeling choices define the range of conditions for which the results in the subsequent sections are considered valid.

System Configuration

Total System Suspension Layout and Assembly Variants

The finite element model represents a single rear suspension corner with a double-wishbone layout. The assembly includes the lower control arm, upper control arm, knuckle, and coil-over shock, all mounted between two chassis reference axes. Axis 1 is placed at the inboard lower-control-arm pivot and taken as the global origin at (0, 0, 0) in. Axis 2 lies at the upper-arm frame joint at approximately (−0.581, 2.70, 0) in. Both axes are oriented along the global z-direction pointing into the wheel well, and the remaining joint locations are defined relative to this coordinate system.

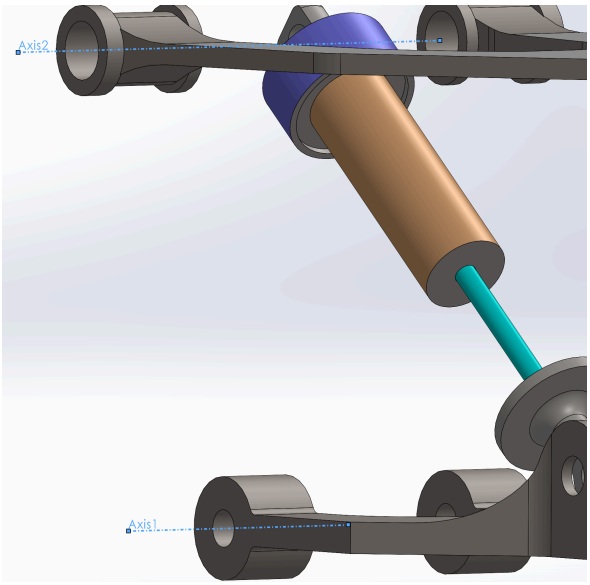

In this configuration, the lower arm connects the two inboard pivots at the frame to the knuckle, forming the primary load path from the wheel hub into the chassis. The upper arm is a shorter, nearly parallel member above the lower arm, providing additional control of camber and lateral positioning. The shock absorber spans between the lower arm and the chassis at an inclined angle, so that vertical motion of the knuckle produces a combination of axial compression and bending in the shock assembly. For the purposes of FEA, the geometry is parameterized by the distances between joint centers (A–G) and the spindle load application point. An isometric view of the full suspension assembly is shown in Figure B, and a dimensioned CAD view summarizing all joint locations and key link and section dimensions is given in Figure C.

Figure B: Rear Suspension Assembly with Axes 1 and 2 Shown

Two assembly configurations are analyzed using this same underlying geometry and joint layout. In the first, the fixed-length shock case, the interface between the shock tube and shock plunger is modeled as a rigid pin connector so that the shock length is effectively locked and no relative axial motion is allowed. In the second, the spring-supported shock case, this pin is replaced by an axial spring connector with a stiffness of 500 lbf/in, permitting compression and extension of the shock under load. All other joints—between the control arms, knuckle, and chassis—are treated identically in both models so that

differences in response can be attributed directly to the change in shock constraint rather than any change in overall layout. Detailed part drawings and dimensions for the arms, knuckle, and shock components are collected in Appendix T for reference.

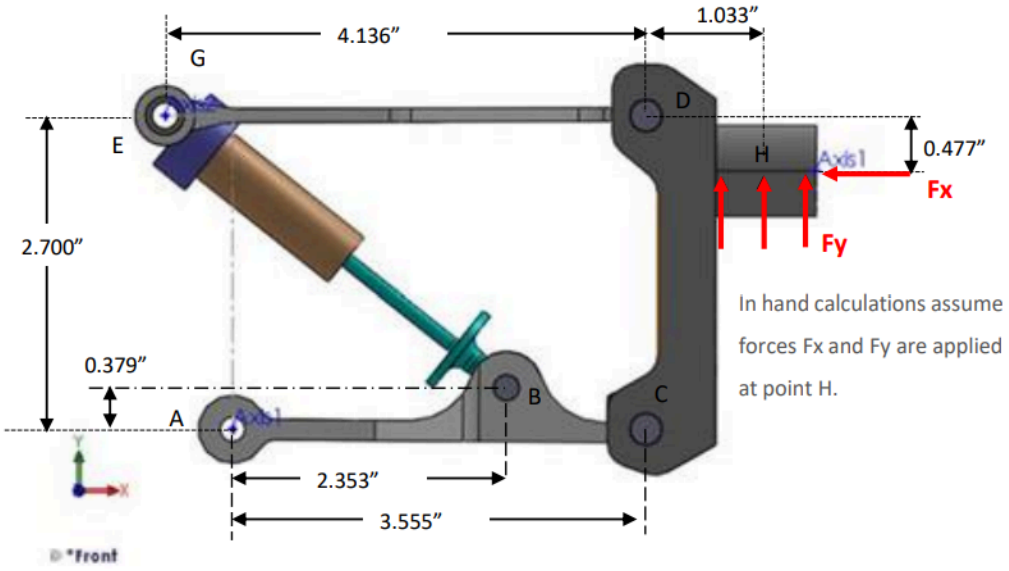

Figure C: Rear Suspension Assembly Major CAD Dimensions

System Properties

Material Definitions and Component Assignments

All parts in the suspension assembly were modeled as homogeneous, linear-elastic, isotropic metals chosen to be representative of realistic automotive components. The upper and lower control arms were assigned AISI 4340 normalized steel, consistent with forged, high-strength suspension arms that need a relatively high elastic modulus and elevated yield and ultimate tensile strengths to withstand repeated cornering and bump loads.

The steering knuckle, shock clamp, shock plunger, and shock tube were modeled using a cast carbon steel material. This choice reflects hardware that would likely be manufactured as castings with more complex geometry, where a moderately ductile material is desirable to transfer loads into the hub and surrounding structure without being overly brittle. In the finite element model, these materials were applied directly to the solid CAD bodies so that stiffness, mass, and strength all followed from the same property sets used during design.

The detailed numerical properties—Young's modulus, shear modulus, Poisson's ratio, mass density, yield strength, and tensile strength—for both AISI 4340 steel and cast carbon steel were taken from SolidWorks. A complete table of the final values used in the analysis is provided in Appendix U.

Connector Modeling and Additional Property Inputs

Because all structural members were represented as 3D solid parts with their full CAD geometry, no separate beam, shell, or thickness definitions were required. Section stiffness and inertia effects are inherently captured by the solid meshes for the control arms, knuckle, and shock components.

In the spring-supported assembly variant, the shock absorber behavior is augmented with an additional connector property: a linear axial spring placed between the shock tube and shock plunger. This connector has a stiffness of 500 lbf/in, derived from a simplified one-dimensional stiffness model of the shock assembly, and links relative axial displacement directly to force. Together, the material assignments and this spring connector define the key input properties that drive the computed stress fields, deflections, and resulting factors of safety in the FEA results presented later in the report.

System Conditions

Assembly-Level Boundary Conditions and Load Case Definition

For both assembly studies, the suspension is constrained to represent its connection to the vehicle frame while allowing realistic in-plane motion of the wheel. The inboard pivots of the lower control arm at A and A′ and the upper control arm pivots at G and G′ are modeled as hinge fixtures. These constraints restrain all three translational degrees of freedom at each frame joint but leave rotation about the pin axis free, mimicking a physical bushing or clevis connection. The shock's upper mount at E is treated in the same way: its origin is fixed in space, but the shock body is free to rotate about the pin axis.

Joints between the control arms and the knuckle are represented as pin connectors rather than fully meshed cylindrical pins. At each of these locations, the connector ties the corresponding cylindrical faces together, enforces coincident rotation about the pin axis, and transmits force and moment between the bodies. This simplifies the mesh while still allowing the correct load path from the knuckle into the arms and then into the frame. The same pin-connector approach is used at the shock-to-lower-arm interface; the only difference between the two assembly variants is whether that interface is rigid (fixed shock) or includes an axial spring (spring-supported shock).

The applied service loads are imposed at the knuckle spindle to approximate a severe combined cornering/braking event. A 100 lbf horizontal force is applied in the global x-direction (positive forward), and a 50 lbf vertical force is applied in the global y-direction (positive upward). These two components are applied concurrently at the wheel-center location, as shown schematically in Figure D, and are transmitted into the arms and frame via the pin connectors and hinge fixtures. In both assembly studies, the same load magnitudes, directions, and application point are used so that differences in stress and deflection can be attributed solely to the shock modeling (rigid vs. spring-supported).

Reaction forces and moments at the frame joints (A, A′, G, G′, and E) are extracted from the FEA and checked against hand-calculated statics (Appendix K and P) to confirm that the global force and moment balance is satisfied. This provides a basic verification that the boundary conditions and load application are consistent and that the FE model is not artificially stiffened or softened by over- or under-constraining the system.

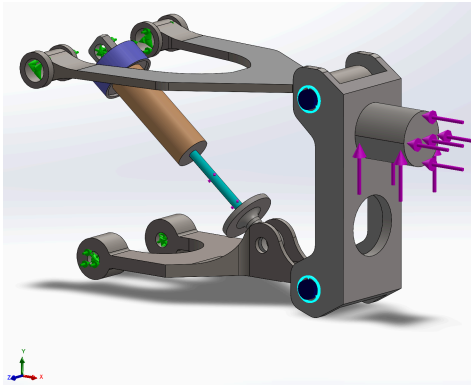

Figure D: Schematic of suspension assembly showing hinge constraints at A/A', G/G', and E and the combined 100 lbf horizontal and 50 lbf vertical load applied at the knuckle spindle.

Local Lower Control Arm Study Conditions

A separate local model of the lower control arm is created to enable more detailed stress analysis and to support the later optimization study. In this standalone model, the lower arm geometry and mesh are retained, but the rest of the suspension is removed and replaced with equivalent boundary conditions derived from the assembly solution.

At the inboard bushing locations (A and A′), the cylindrical pin bores are constrained with hinge-like fixtures that fix translations but allow rotation about the pin axis, replicating the same kinematic condition used in the full assembly. At the knuckle-side bores (B and B′, C and C′), the contact with the knuckle is replaced by remote loads and constraints that reproduce the reaction forces and moments transferred through those joints in the assembly model. In practice, this is implemented by coupling the motion of nodes around each bore and applying the resultant forces and, if needed, bending moments to the coupled region so that the local stress state in the fillets and ligaments is consistent with the assembly-level behavior.

The same global load case—100 lbf horizontal and 50 lbf vertical applied at the wheel center—is implicitly carried into the local model through these equivalent reactions, so no additional external forces are directly applied to the lower arm. The coordinate system, material properties, and linear-elastic assumptions all match those of the assembly simulations. By isolating the lower arm with appropriately transferred boundary conditions, this local model provides higher resolution of the critical fillet regions while keeping computation time manageable and avoiding remeshing the entire suspension assembly for each design iteration.

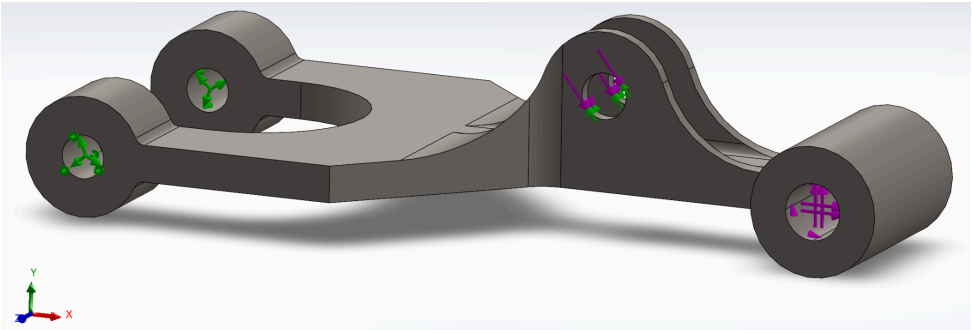

Figure E: Standalone lower control arm model showing hinge constraints at A/A' and equivalent reaction loads applied at the knuckle-side bores.

System Discretization

Element Formulation and Global Mesh Settings

The suspension components were meshed using SolidWorks Simulation's *high-quality* curvature-based tetrahedral solid elements. The identical meshing approach was applied to both assembly analyses—the "fixed" shock configuration and the spring-supported configuration—so that any change in response is due only to the boundary conditions and the shock connector, not to differences in element formulation.

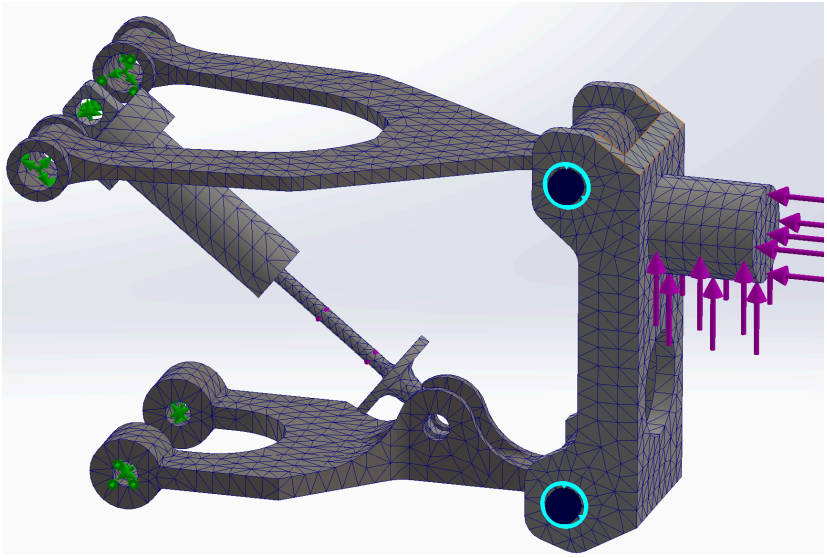

Figure F: Rear Suspension Assembly with Global Mesh

A global target element size of about 0.090 in was assigned to all parts. Where possible, contacts between components were modeled using the standard compatible mesh, and the software's automatic refinement along contact regions was used to maintain reasonable element aspect ratios and prevent highly distorted elements. This produced a mesh that is fine enough near interfaces while remaining efficient elsewhere. An overview of the final 3D mesh and overall element distribution is presented in Figure F.

Local Mesh Refinement

Additional mesh controls were applied in regions where large stress gradients or tight curvature are expected. In the full assembly, a refined element size of 0.070 in was specified at the shock tube–plunger contact surfaces that transfer load through the spring or pin connector.

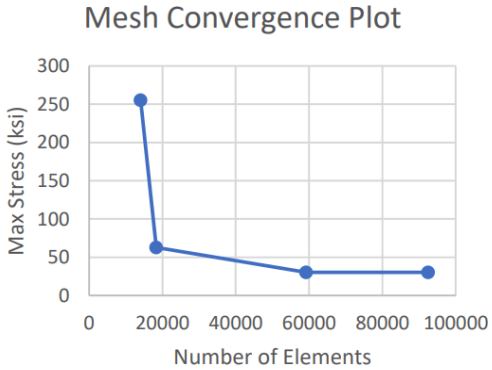

For the standalone lower-control-arm model, further local refinement was introduced around the inner radii of the arm. These controls ensure that the mesh accurately resolves the bending-driven stress concentration in the knuckle-side fillets, which ultimately governs the minimum factor of safety for the arm. With these refinements in place, the final mesh exhibits smooth transitions in element size from the highly refined zones into the coarser bulk regions, avoiding abrupt jumps in element dimensions.

Mesh Convergence Study

A manual mesh convergence study was carried out on the lower-control-arm model to confirm that the mesh density is sufficient for the final design. The primary convergence metric was the peak von Mises stress at the critical fillet in the lower arm, and the y-direction deflection at the outer knuckle joint was monitored as a secondary quantity.

Beginning with a relatively coarse mesh, the local element size in the critical fillet region was gradually decreased over several refinement steps, while the global mesh settings were kept constant. For each refinement level, the maximum von Mises stress and the corresponding nodal displacement were recorded.

Once the local element size was reduced below approximately 0.070 in, the change in peak von Mises stress between successive refinements dropped to less than 4%, and the variation in y-deflection stayed within a similar range. The trends of peak stress and deflection versus total element count are plotted in Figure G. The mesh ultimately used for all reported results corresponds to the finest refinement level that satisfies a <5% convergence tolerance, while still keeping the overall element count manageable for iterative analysis.

Verification and Validation

Statics-Based Joint Reaction Verification

To verify that the boundary conditions and applied loads in the assembly model were implemented correctly, a statics check of the joint reactions was carried out. Free-body diagrams of the knuckle and lower control arm were drawn using the same 100 lbf horizontal and 50 lbf vertical forces applied at the spindle in the FEA model. Using equilibrium equations and standard Mechanics of Materials relations, the reaction forces at the frame pivots (A, A′, G, G′) and at the shock mount E were solved analytically.

These hand-calculated reactions were then compared directly to the reaction forces reported by SolidWorks Simulation at the corresponding hinge fixtures and connectors. The vertical load path from the knuckle into the lower arm and shock, and the horizontal load path into the arms and frame, were checked component by component. The FEA reactions closely matched the analytical values, with only small percentage differences, confirming that the overall load balance and support conditions in the model are consistent with the intended physical system. The reactions used in the subsequent shock-absorber modeling are summarized in Table 2.

Table 2: Joint Reactions

Location	Comonet	SWS	Hand	Description

One-Dimensional Shock-Absorber Stiffness Model

A simplified one-dimensional spring model was developed to justify the axial stiffness assigned to the shock connector in the spring-supported assembly. Using the joint reactions from the statics verification, the axial force carried by the shock under the combined 100 lbf horizontal and 50 lbf vertical load was extracted. The change in shock length associated with the corresponding knuckle motion was then estimated from the suspension geometry.

By relating the axial force in the shock to the estimated deflection through Hooke's law, an equivalent linear spring stiffness of 500 lbf/in was obtained. This stiffness value was implemented as the axial spring connector between the shock tube and plunger in the FEA model. When the 1D spring model is loaded with the same spindle displacement as in the FE simulations, it predicts shock forces that are consistent with the connector forces reported by SolidWorks Simulation. This agreement supports the use of the 500 lbf/in spring constant as a reasonable representation of the shock's in-plane stiffness for the purposes of this study.

Table 3: Stiffness Model Hand Calculations (Appendix N)

	$K_{shocktube}$	$K_{plunger}$	δ_1	$K_{shocktube}$	$K_{plunger}$	K_{spring}	δ_2

Case	Variation 1: Fixed	Variation 1: Fixed	Variation 1: Fixed	Variation 2: Spring	Variation 2: Spring	Variation 2: Spring	Variation 2: Spring
Value (lbf/in)	$1.36(10^6)$	$2.93(10^5)$	$-4.19(10^{-4})$ (in)	$1.36(10^6)$	$2.93(10^5)$	500	-0.202 (in)

Conceptual Experimental Validation

In addition to the analytical checks, a conceptual experimental plan was outlined to show how the numerical model could be validated against physical measurements. The suspension corner could be mounted to a rigid test frame with physical hinges at A/A′, G/G′, and E that reproduce the same constraints used in the FE model. The knuckle spindle would then be loaded with the combined horizontal and vertical forces using a lever arm or test machine capable of reproducing the 100 lbf and 50 lbf components.

Measurements could be taken using dial indicators at the spindle and at the shock clamp to record vertical deflection and shock compression, and a strain-gauge rosette bonded near the B–B′ fillet on the lower control arm could provide local strain data to convert to stress. If the experimentally measured peak stress, von Mises stress at the gauge location, spindle deflection, and shock compression all agree with the FEA predictions within roughly 5–10% in the elastic range, the model's boundary conditions, loading, and stiffness representation would be considered adequately validated for this linear-static analysis. Taken together, the statics-based reaction check, the Mechanics of Materials relationships, the 1D spring model, and the proposed experimental comparison provide a coherent basis for trusting the lower-control-arm simulations before drawing design conclusions from the FEA.

Results

Overview of FEA Studies and Primary Outputs

Finite element results are reported for three configurations:

1. The full double-wishbone assembly with a fixed-length shock modeled as a rigid pin between the shock tube and plunger.

2. The same assembly with a 500 lbf/in axial spring connector replacing that pin at the shock, allowing extension and compression.

3. A standalone lower-control-arm model with equivalent boundary conditions taken from the assembly reactions.

For each case, the primary quantities of interest are:

- The maximum von Mises stress in the lower control arm, which governs the factor of safety against yielding.
- The peak x-normal stress, σ_x, in the critical fillet region at the knuckle-side bores (sections B–B′ and C–C′).
- The maximum vertical displacement in the global y-direction, evaluated at the knuckle spindle and, for the assembly models, along the shock axis.

These scalar results are summarized in Table 4, while the full stress and displacement contours for each study are provided in the corresponding appendices (von Mises and displacement plots for the fixed and spring-supported assemblies and for the standalone lower arm). The finalized deflection and stress contour plots for all three studies are provided in Appendices A–J.

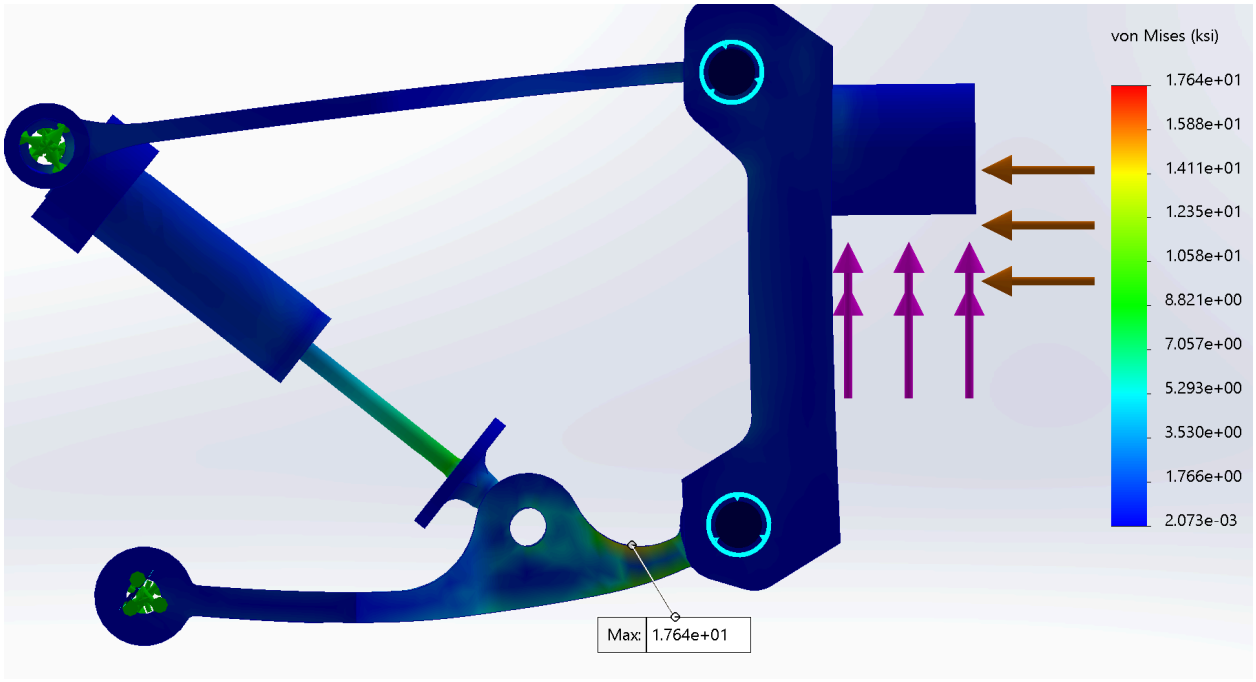

Figure H: Double Wishbone Study - Fixed: von Mises Plot

Table 4: Full Simulation Results

Study Type	Max vonMises (kis)	Absolute x-normal stress (kis)	Max y-displacement (in)	Factor of Safety
Wishbone - fixed	17.64	-14.57	0.0041	3.7
Wishbone - Spring	17.65	-14.57	0.4504	3
Lower Control Arm	18.41	-15.23	0.00255	5.5

The two assembly cases show that changing the shock from a rigid link to a 500 lbf/in spring produces a

large increase in vertical deflection—primarily through shock extension—while leaving the peak stresses in the lower arm essentially unchanged. The standalone lower-arm study predicts slightly higher von Mises and σ_x values at the critical fillet than the assembly models, as expected from the more refined local mesh and direct application of the equivalent reaction loads. In all cases, the resulting stresses remain below the yield strength of the material with an acceptable factor of safety given the 3.5 target used throughout the project.

Lower Control Arm Optimization Results (Bonus)

In addition to the baseline lower-arm analysis, a SolidWorks design optimization study was carried out on the standalone lower-control-arm model. The objective of this study was to reduce the mass of the arm while still satisfying the strength and stiffness requirements under the same equivalent loading derived from the assembly. The optimization treated selected geometric dimensions on the arm (such as wall thicknesses and local cross-sectional features) as design variables, constrained the minimum factor of safety in the critical knuckle-side fillet to remain at or above 3.5, and enforced basic geometric and manufacturability limits.

The resulting optimized geometry preserves the controlling fillet shape at the knuckle bores but removes material from less critical regions of the arm, especially in thicker mid-span sections and secondary ribs, where stress levels are lower. The optimized design therefore achieves a lighter lower control arm while keeping the peak von Mises and σ_x stresses in the critical region comparable to the baseline design and maintaining small vertical deflections at the knuckle. Detailed dimensions and quantitative weight and stress comparisons for the baseline and optimized arms are compiled in Appendix S.

Discussion

Interpretation of Suspension Response and Design Tradeoffs

In all three models, the governing feature is the lower control arm fillet at the knuckle-side bores B–B′ and C–C–′, where the FEA consistently reports the highest von Mises and σ_x stresses from the combined knuckle reactions and strut load. In the full assembly, the fixed-shock configuration behaves as a very stiff system: spindle deflection is small, and the shock length does not change, so most of the vertical compliance is carried by the arm geometry itself.

Switching to the spring-supported configuration makes the suspension much more compliant at both the spindle and the shock, but the critical fillet does not change and the peak stresses in the lower arm remain very close to those in the fixed-shock case. The main effect of adding the 500 lbf/in spring is therefore to increase vertical motion at the spindle and shock rather than to shift or amplify the critical lower-arm stress. The standalone lower-control-arm model is especially useful here because it isolates this fillet, reproduces the hand-calculated reactions and deflections, and allows geometry changes to be evaluated without remeshing the full suspension. In that local model, the maximum deflection of the arm itself remains small, reinforcing that most of the added compliance in the spring-supported assembly comes from the shock flexibility, not from the lower arm.

The optimized lower-control-arm geometry retains the same knuckle-side fillet as the controlling region but reduces arm mass by approximately 26.96% while still maintaining a minimum factor of safety of

3.515 relative to the AISI 4340 yield strength. This captures the central benefit of the optimization: a meaningful reduction in unsprung mass so the suspension can track the road more easily, with essentially no penalty in local stress or overall stiffness. The corresponding drawback is that each candidate geometry must be meshed, constrained, and loaded in a strictly consistent way—small shifts in local element size, contact setup, or boundary conditions can otherwise produce misleading changes in the reported factor of safety.

Model Limitations and Recommended Next Steps

These results must be interpreted within the limits of the current model. The analysis is based on a single, in-plane, linear-static load case with ideal pinned joints, uniform material properties, and a simplified linear spring representation of the shock. A real suspension will experience dynamic braking and cornering, out-of-plane loading, bushing compliance, friction effects, and manufacturing details such as welds and small radius variations that can raise local stresses and affect fatigue performance.

As a result, this FEA should be treated as an elastic design and comparison tool that shows the optimized lower control arm is promising and clarifies the influence of the fixed versus spring-supported shock configurations. Final design decisions should still be supported by additional load cases, a fatigue assessment, and targeted physical testing to confirm both stress levels and deflections under more realistic service conditions.

Conclusion

This project applied a sequence of assembly-level and local finite element studies, supported by hand calculations and a mesh-convergence check, to assess a double-wishbone rear suspension under a severe in-plane load case. Across all configurations, the knuckle-side fillet of the lower control arm remained the critical region, and the simulations showed that both the baseline and optimized arms provide sufficient stiffness and maintain a factor of safety above the design requirement.

The standalone lower-control-arm model proved especially effective for refining this critical geometry without repeatedly remeshing the entire assembly, enabling a 26.96% reduction in unsprung mass while preserving structural performance and keeping the minimum factor of safety at 3.515. Overall, the study illustrates how a carefully verified FE workflow—combining system-level and local models—can guide weight-optimized suspension designs that still meet strength and deflection targets.

Appendix

Appendix A: Double Wishbone Study - Fixed: von Mises Plot

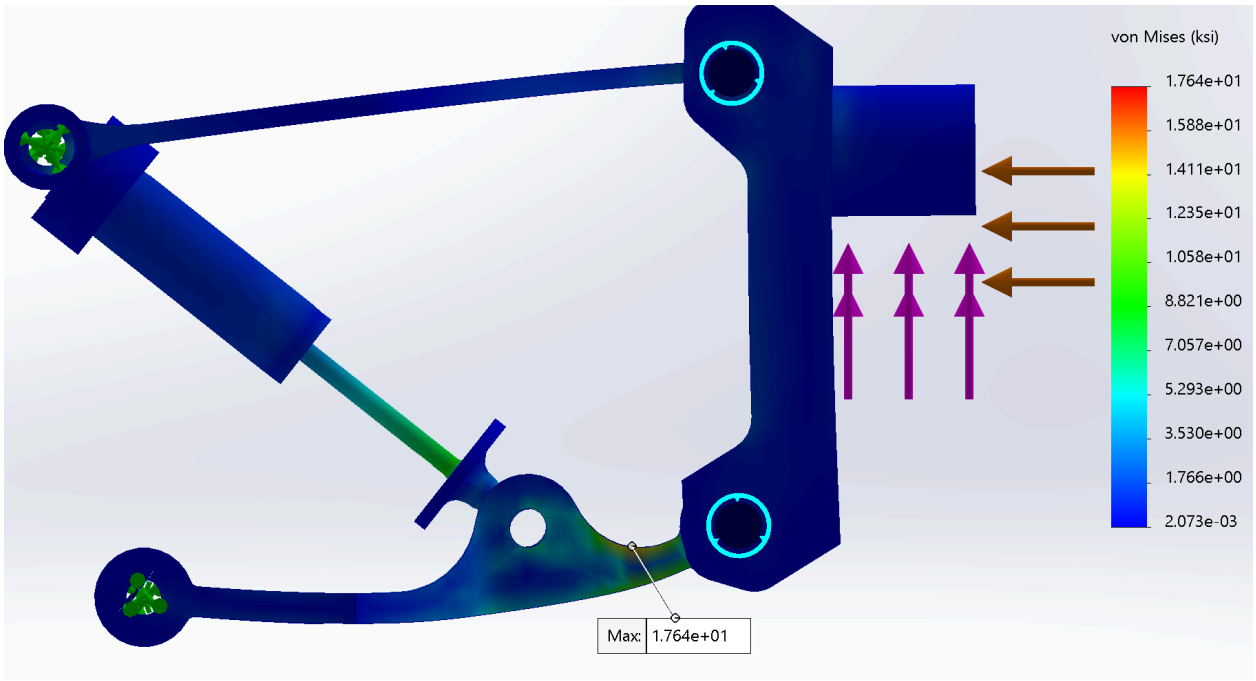

Appendix B: Double Wishbone Study - Fixed: σ_x Stress Plot

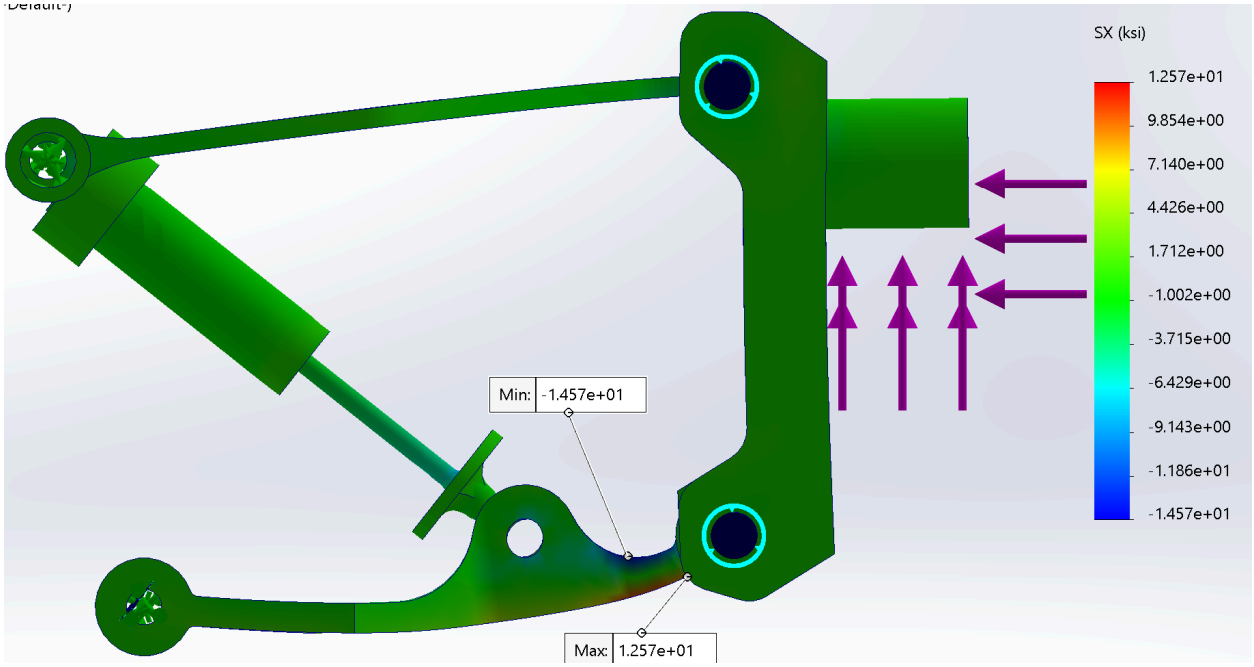

Appendix C: Double Wishbone Study - Fixed: Y - Displacement Plot

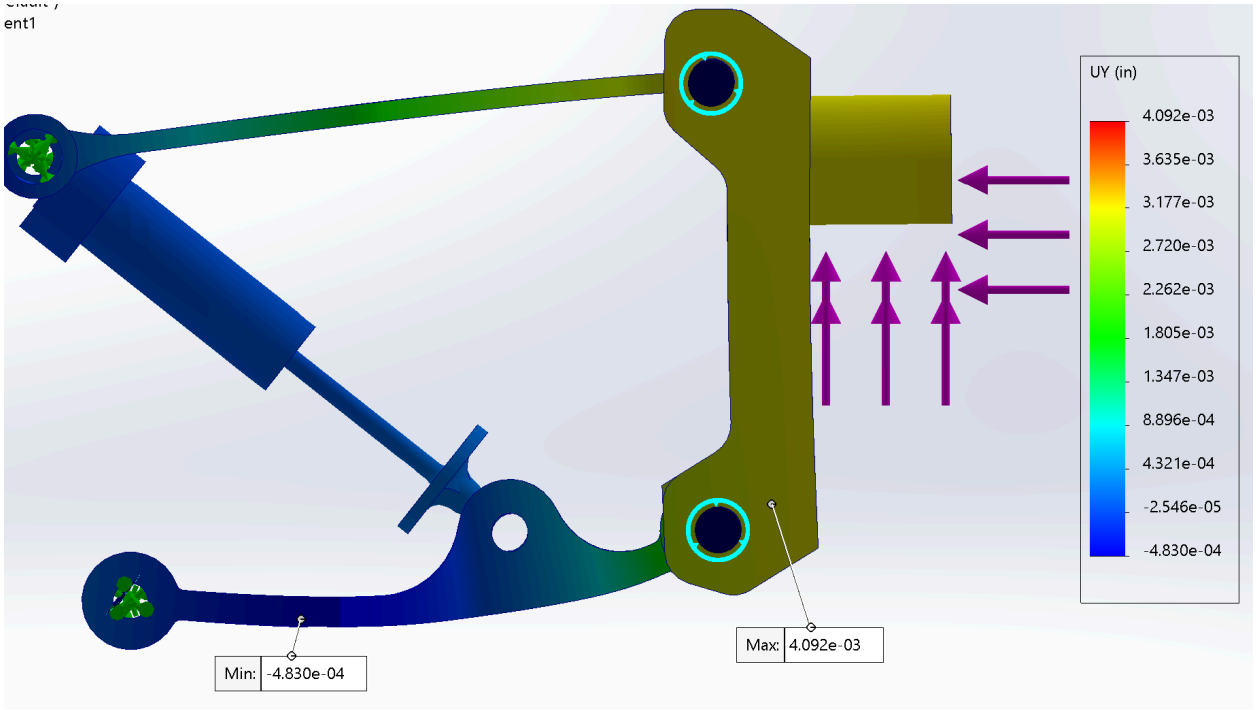

Appendix D: Double Wishbone Study - Spring: von Mises Plot

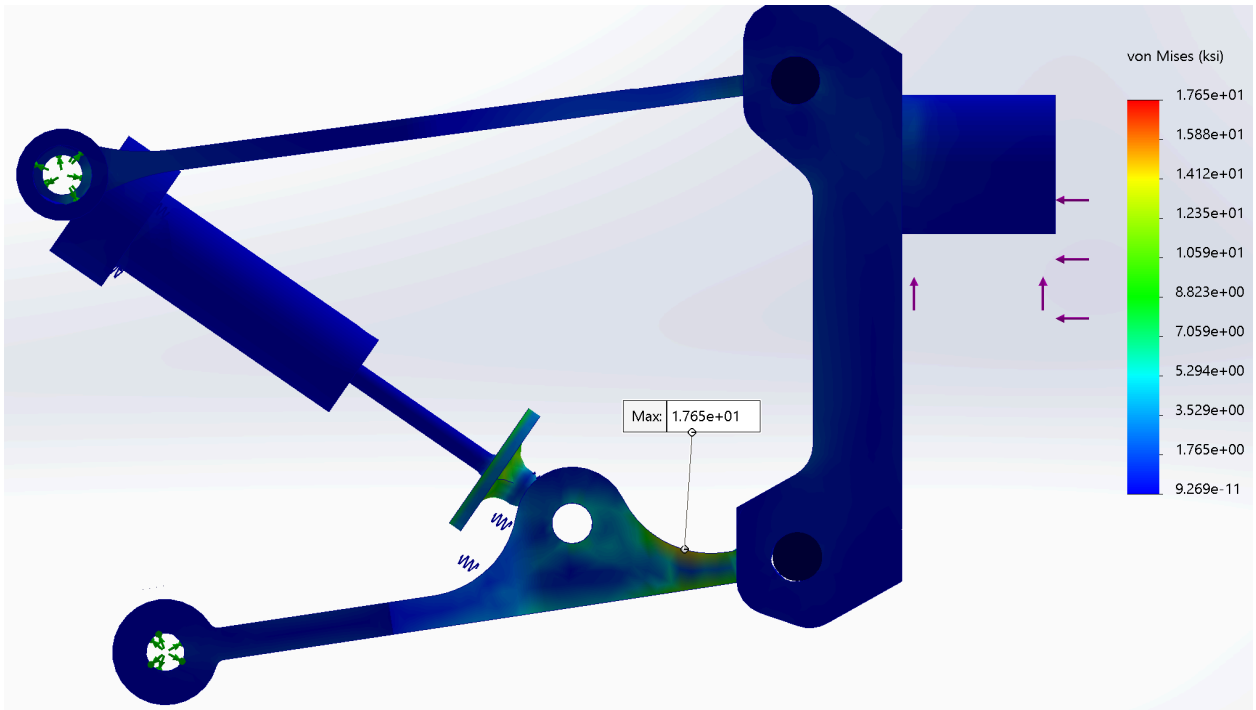

Appendix E: Double Wishbone Study - Spring: σ_x Stress Plot

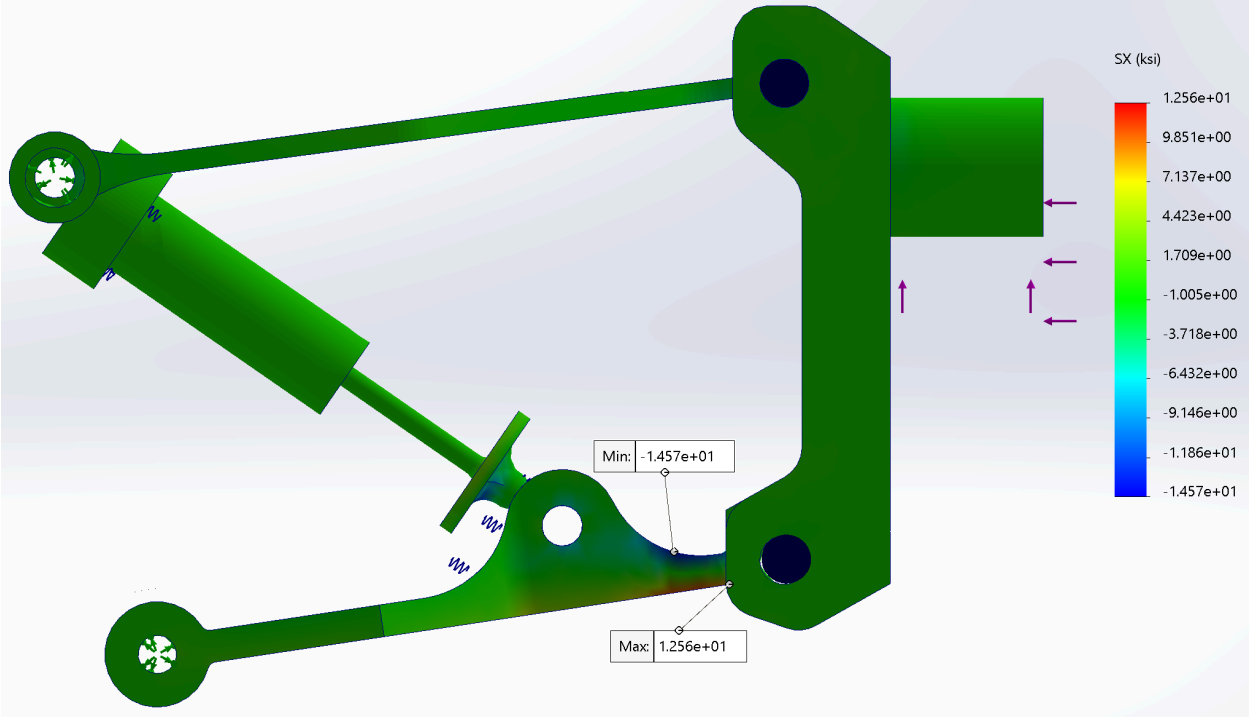

Appendix F: Double Wishbone Study - Spring: Y - Displacement Plot

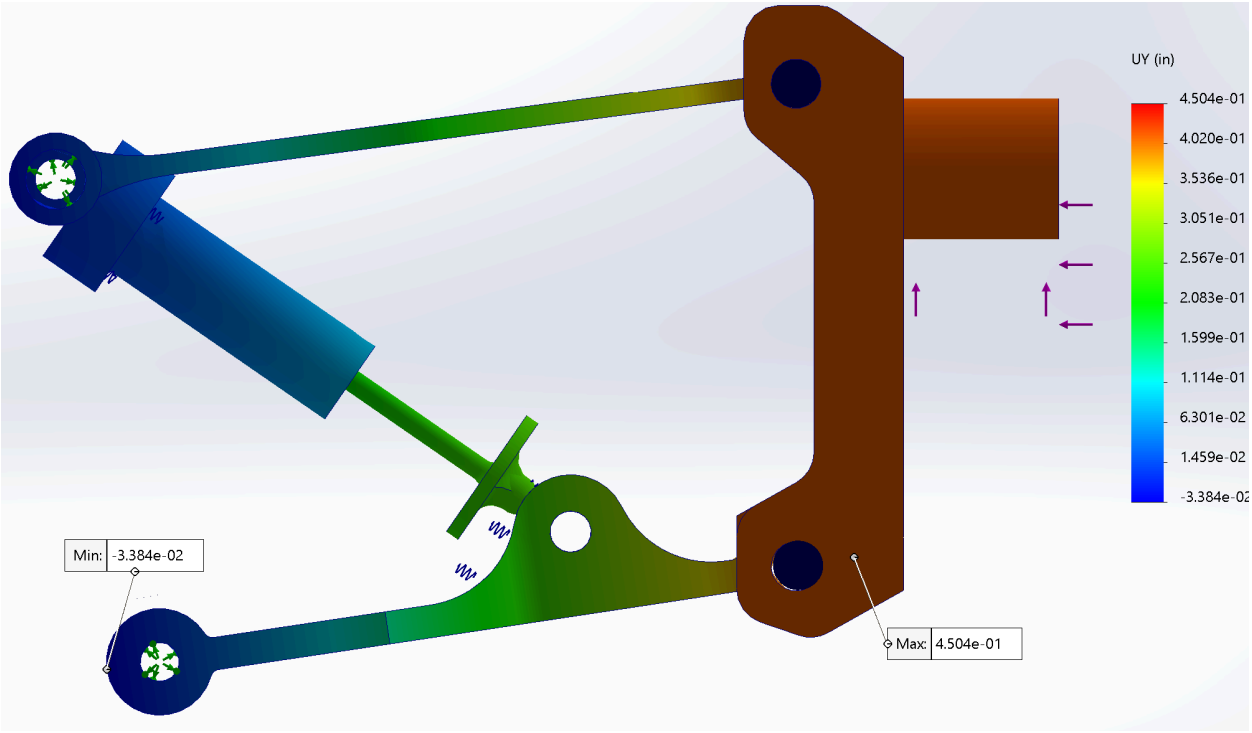

Appendix G: Lower Arm Study: von Mises Plot

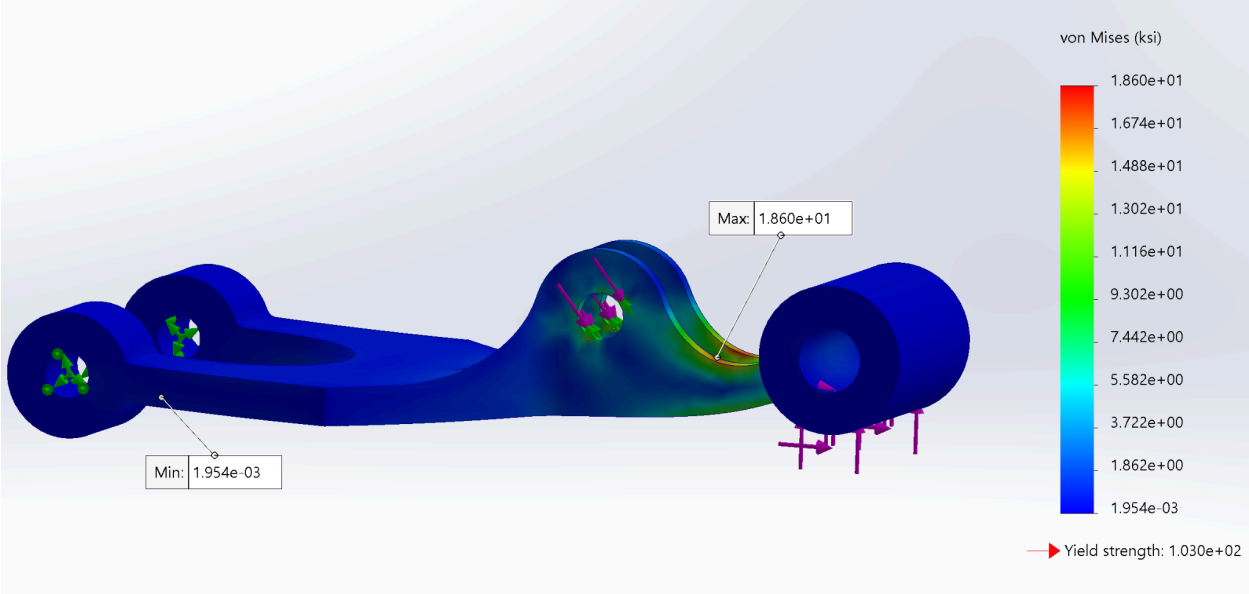

Appendix H: Lower Arm Study:σ_x Stress Plot

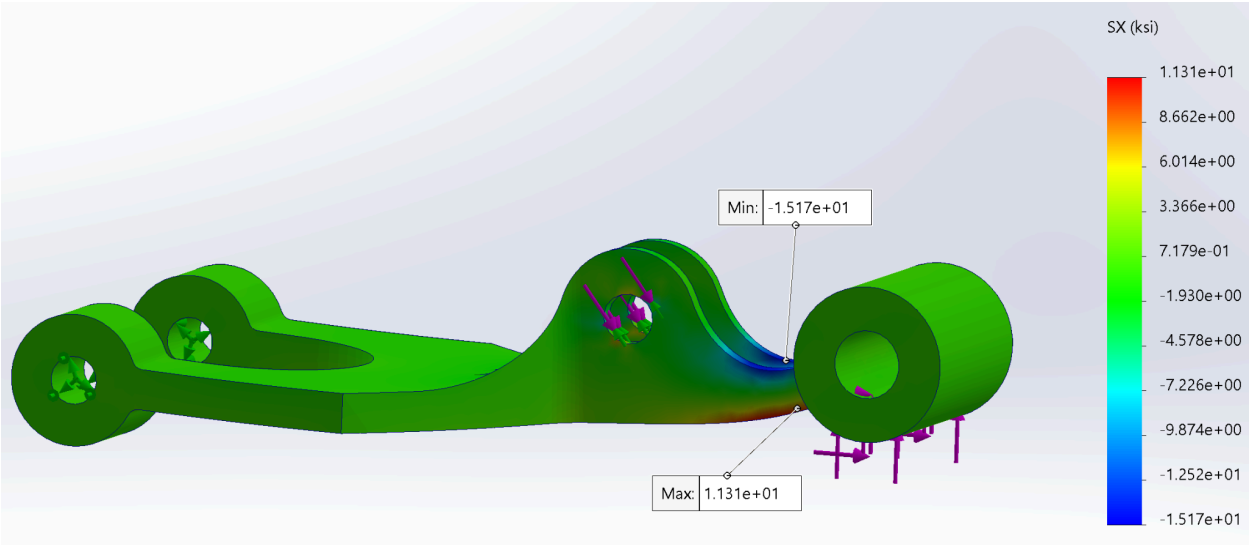

Appendix I: Lower Arm Study: Y - Displacement Plot

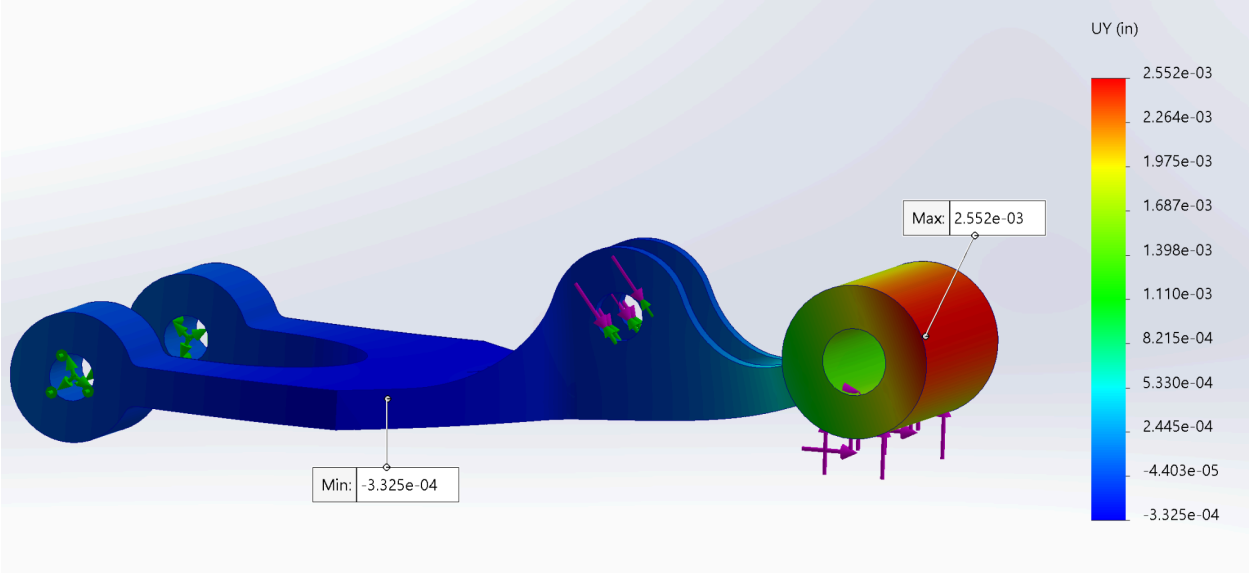

Appendix J: Lower Arm Study: Factor of Safety Plot

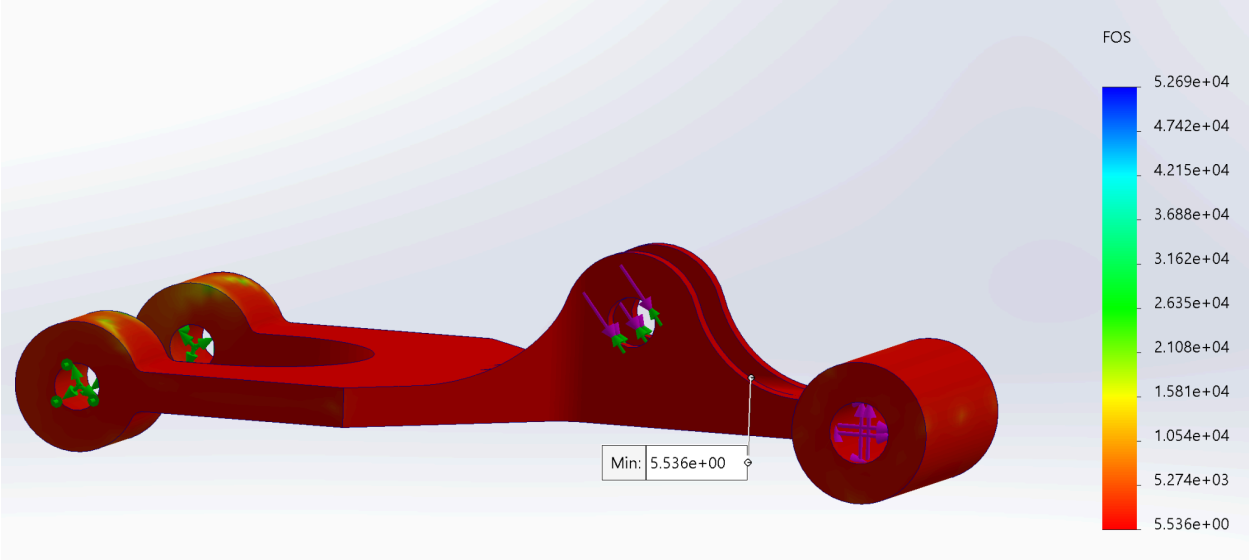

Appendix K: FBD of System

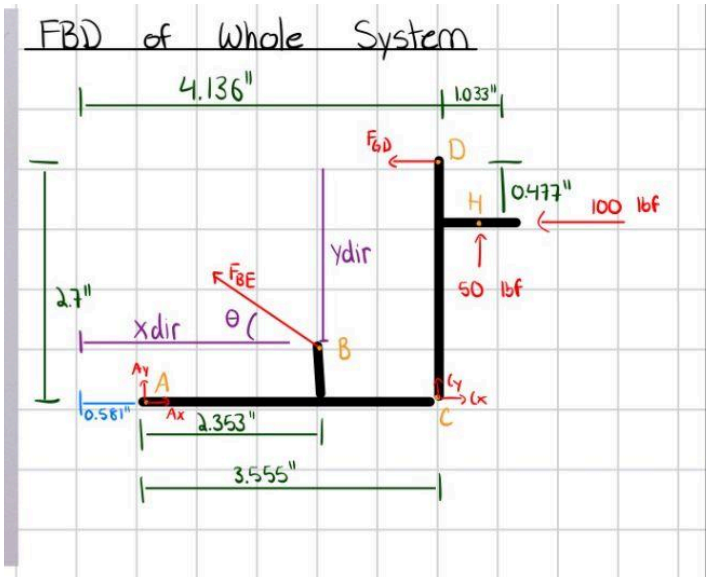

Appendix L: FBD of Knuckles

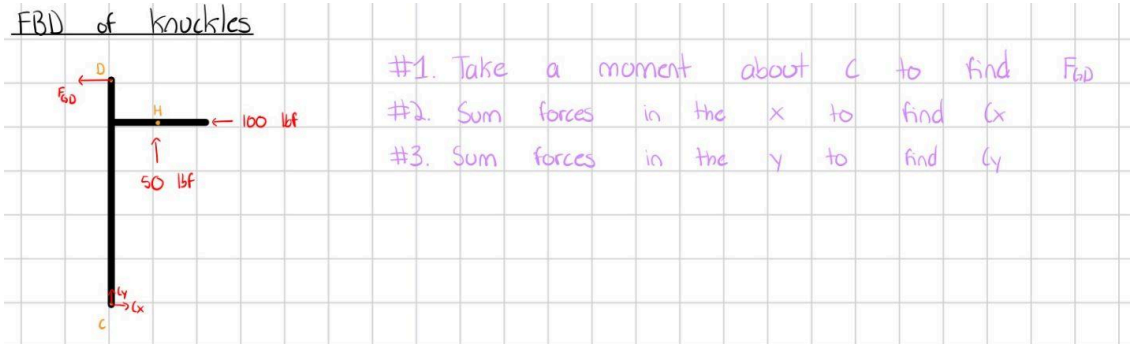

Appendix M: FBD of Lower Arm

Appendix N: Variation - Fixed: Set up

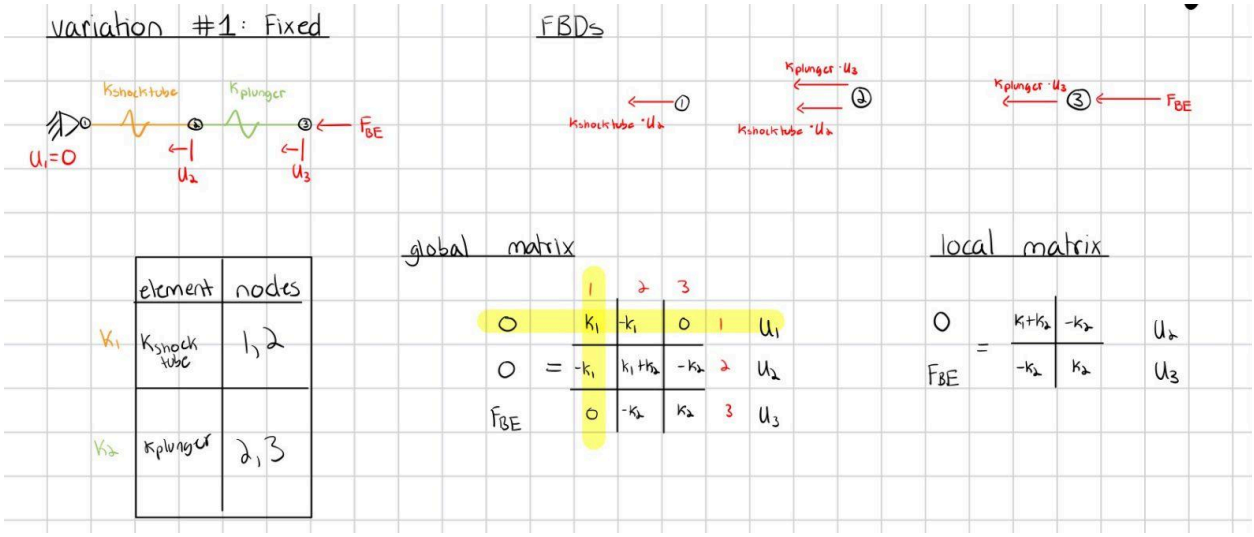

Appendix O: Variation - Springs: Set up

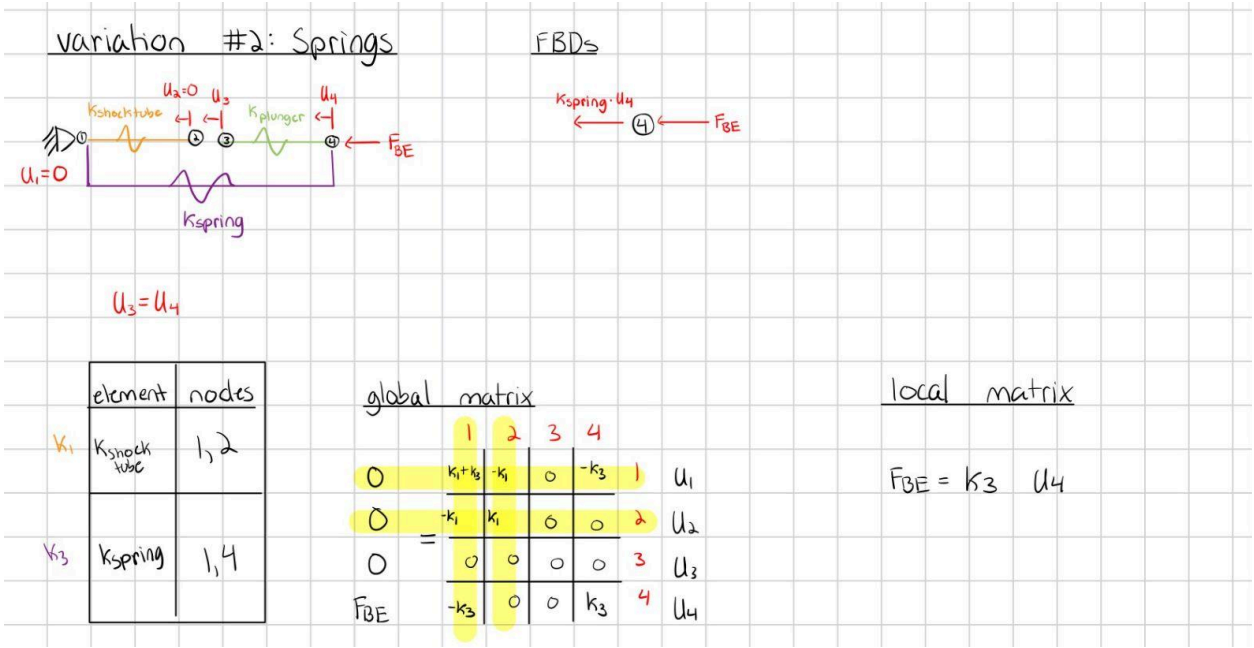

Appendix P: Mechanics of Materials Calculations (hand calculations) - Section 1

Problem 2: Internal Forces Statics:

$xdir := (4.136 - 3.555) + 2.353 = 2.934$ $\qquad Fx := 100\ lbf$

$ydir := (2.7 - 0.379) = 2.321$ $\qquad Fy := 50\ lbf$

$hypotenuse := \sqrt{(xdir^2 + ydir^2)} = 3.741$

$\theta := \operatorname{atan}\left(\frac{ydir}{xdir}\right) = 38.346\ deg$

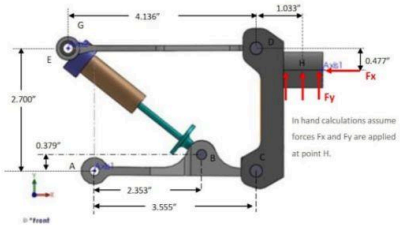

For Knuckle Forces:

$\sum M_C = Fy \cdot 1.033 + Fx \cdot 2.223 - F_{GD} \cdot 2.7 = 0$

$F_{GD} := \frac{(Fy \cdot 1.033 + Fx \cdot 2.223)}{2.7} = 101.463\ lbf$

$FXnet = F_{GD} - Fx + Cx = 0$ $\qquad Cx := Fx - F_{GD} = -1.463\ lbf$

$FYnet = Cy + Fy = 0$ $\qquad Cy := 0 - Fy = -50\ lbf$

For Lower Control Arm Forces:

$\Sigma M_A = -Cy \cdot 3.555 - F_{BE} \cdot 2.353 \cdot cos(\theta) - F_{BE} \cdot 0.379 \cdot sin(\theta) = 0$

$F_{BE} := \frac{(-Cy \cdot 3.555)}{(2.353 \cdot \sin(\theta) + 0.379 \cdot \cos(\theta))} = 101.162\ lbf$

$FXnet = Cx - F_{BE} \cdot cos(\theta) + Ax = 0$ $\qquad Ax := F_{BE} \cdot \cos(\theta) - Cx = 80.802\ lbf$

$FYnet = Cy + F_{BE} \cdot sin(\theta) + Ay = 0$ $\qquad Ay := -Cy - F_{BE} \cdot \sin(\theta) = -12.763\ lbf$

Table of Forces:

$F_{BE} = 101.162\ lbf$

$Ax = 80.802\ lbf$	$Cx = -1.463\ lbf$	$Ex := F_{BE} \cdot \cos(\theta) = 79.339\ lbf$
$Ay = -12.763\ lbf$	$Cy = -50\ lbf$	$Ey := F_{BE} \cdot \sin(\theta) = 62.763\ lbf$
$Bx := F_{BE} \cdot \cos(\theta) = 79.339\ lbf$	$Dx := F_{GD} = 101.463\ lbf$	$Gx := F_{GD} = 101.463\ lbf$
$By := F_{BE} \cdot \sin(\theta) = 62.763\ lbf$	$Dy := 0$	$Gy := 0$

Appendix Q: Mechanics of Materials Calculations (hand calculations) - Section 2

Problem 3: 1D FEA:

Element Stiffness

$E := 200\ GPa$

$A_{shocktube} := \pi \cdot \frac{\left(0.49606299^2 - 0.39606299^2\right)}{4}\ in^2 = 0.07\ in^2$

$A_{plunger} := \pi \cdot \frac{0.125^2}{4}\ in^2 = 0.012\ in^2$

$L_{shocktube} := 1.496\ in$

$L_{plunger} := 1.215\ in$

$k_{shocktube} := \frac{\left(E \cdot A_{shocktube}\right)}{L_{shocktube}} = \left(1.359 \cdot 10^6\right)\ \frac{lbf}{in}$

$k_{plunger} := \frac{\left(E \cdot A_{plunger}\right)}{L_{plunger}} = \left(2.93 \cdot 10^5\right)\ \frac{lbf}{in}$

$k_{spring} := 500\ \frac{lbf}{in}$

Variation 1: Fixed

$k_1 := \begin{bmatrix} k_{shocktube} \\ k_{plunger} \end{bmatrix} = \begin{bmatrix} 1.359 \cdot 10^6 \\ 2.93 \cdot 10^5 \end{bmatrix}\ \frac{lbf}{in}$

$K_1 := \begin{bmatrix} k_{1_1} + k_{1_2} & -k_{1_2} \\ -k_{1_2} & k_{1_2} \end{bmatrix} = \begin{bmatrix} 1.652 \cdot 10^6 & -2.93 \cdot 10^5 \\ -2.93 \cdot 10^5 & 2.93 \cdot 10^5 \end{bmatrix}\ \frac{lbf}{in}$

$f_1 := \begin{bmatrix} 0 \\ -F_{BE} \end{bmatrix} = \begin{bmatrix} 0 \\ -101.162 \end{bmatrix}\ lbf$

$U_1 := K_1^{-1} \cdot f_1 = \begin{bmatrix} -0.000074460054 \\ -0.000419742254 \end{bmatrix}\ in$

Variation 2: Springs

$k_2 := \begin{bmatrix} k_{shocktube} \\ k_{plunger} \\ k_{spring} \end{bmatrix} = \begin{bmatrix} 1.359 \cdot 10^6 \\ 2.93 \cdot 10^5 \\ 500 \end{bmatrix}\ \frac{lbf}{in}$

Appendix R: Mechanics of Materials Calculations (hand calculations) - Section 3

$K_2 := k_{2_3} = 500\ \frac{lbf}{in}$

$f_2 := -F_{BE} = -101.162\ lbf$

$U_2 := K_2^{-1} \cdot f_2 = -0.202324664426\ in$

Appendix S: Lower Arm Design Study Results

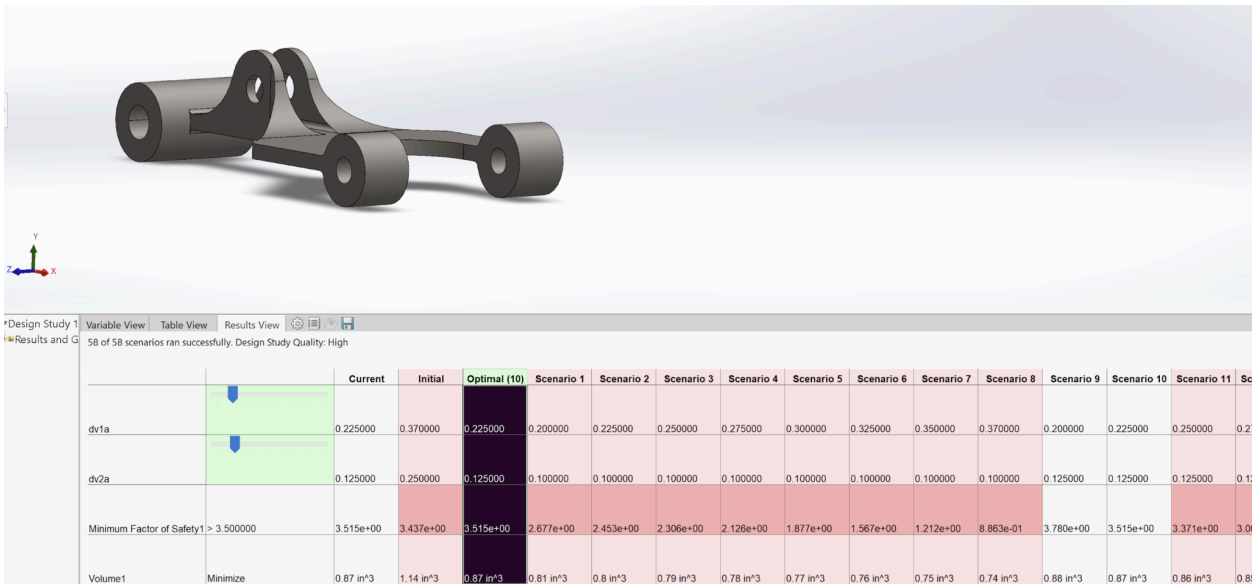

Design Study 1 | Variable View | Table View | Results View

Results and G | 58 of 58 scenarios ran successfully. Design Study Quality: High

			Current	Initial	Optimal (10)	Scenario 1	Scenario 2	Scenario 3	Scenario 4	Scenario 5	Scenario 6	Scenario 7	Scenario 8	Scenario 9	Scenario 10	Scenario 11	Sc
dv1a			0.225000	0.370000	0.225000	0.200000	0.225000	0.250000	0.275000	0.300000	0.325000	0.350000	0.370000	0.200000	0.225000	0.250000	0.2
dv2a			0.125000	0.250000	0.125000	0.100000	0.100000	0.100000	0.100000	0.100000	0.100000	0.100000	0.100000	0.125000	0.125000	0.125000	0.1
Minimum Factor of Safety1	>	3.500000	3.515e+00	3.437e+00	3.515e+00	2.677e+00	2.453e+00	2.306e+00	2.126e+00	1.877e+00	1.567e+00	1.212e+00	8.863e-01	3.780e+00	3.515e+00	3.371e+00	3.0
Volume1	Minimize		0.87 in^3	1.14 in^3	0.87 in^3	0.81 in^3	0.8 in^3	0.79 in^3	0.78 in^3	0.77 in^3	0.76 in^3	0.75 in^3	0.74 in^3	0.88 in^3	0.87 in^3	0.86 in^3	0.8

Appendix T: Lower Control Arm Part Drawing

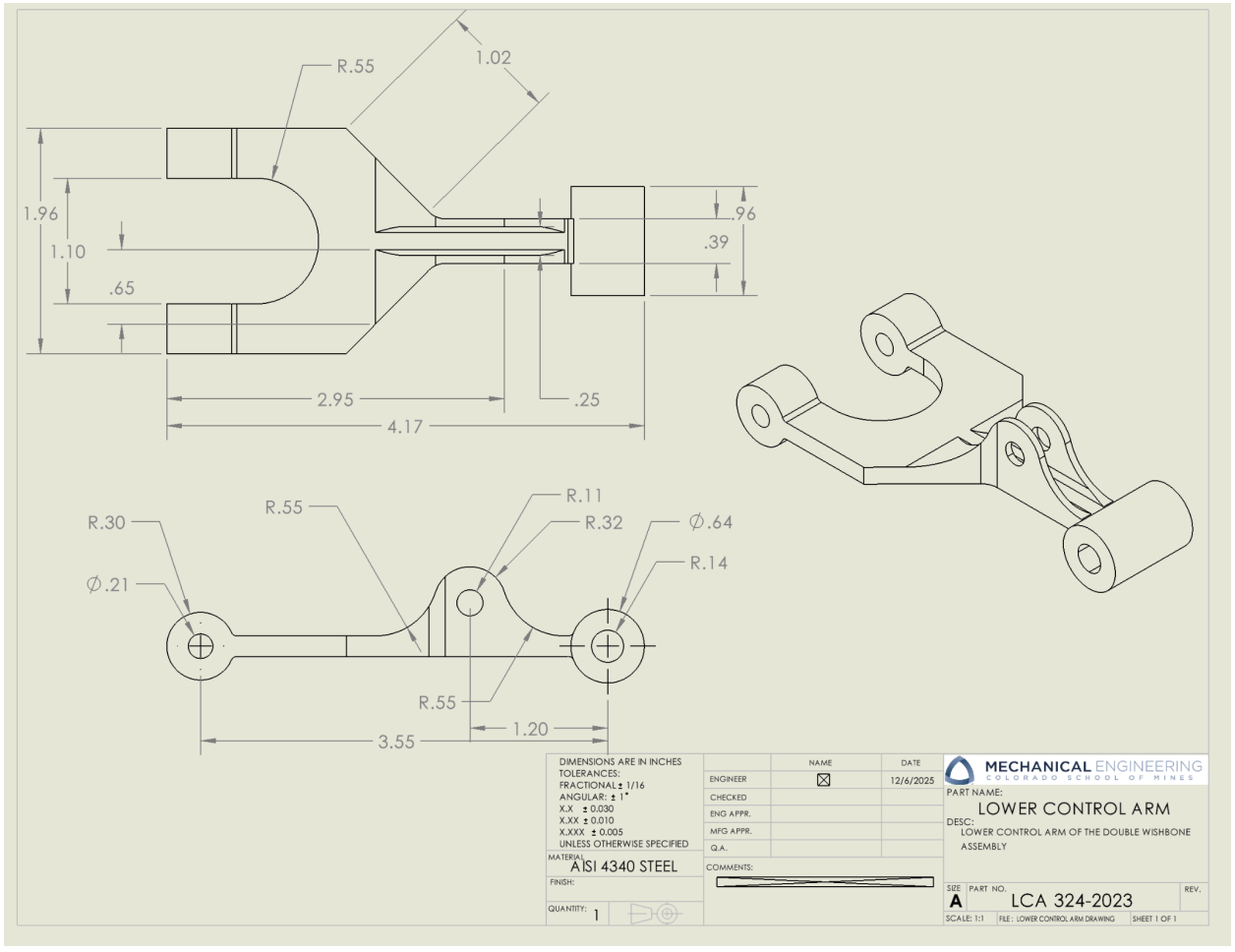

Appendix U: System Properties Table

Property	AISI 4340 Steel	Cast Carbon Steel	Units
Elastic Modulus	29,732,736.22	29,007,547.53	psi
Yield Strength	102,976.79	35,993.73	psi
Tensile Strength	160,991.89	69,987.82	psi
Poisson's Ratio	0.32	0.32	N/A
Shear Modulus	11,603,019.01	11,022,868.06	Psi
Mass Density	0.2836	0.2818	lb/in^3